Journal of Petroleum Science and Engineering 220 (2023) 111170

Contents lists available at ScienceDirect

Journal of Petroleum Science and Engineering

journal homepage: www.elsevier.com/locate/petrol

The heterogeneity of petrophysical and elastic properties in carbonate rocks controlled by strike-slip fault: A case study from yangjikan outcrop in the tarim basin

Fei Gong [a,b], Yichen Song [b], Lianbo Zeng [b,*], Guangui Zou [a]

[a] College of Geoscience and Surveying Engineering, China University of Mining and Technology, Beijing, China
[b] State Key Laboratory of Petroleum Resources and Prospecting, China University of Petroleum, Beijing, China

ARTICLE INFO

Keywords:
Carbonate outcrops
Strike-slip fault
The pore network architectures
Petrophysical and elastic properties
Heterogeneity

ABSTRACT

The petrophysical and elastic properties of the carbonate rocks controlled by strike-slip fault are still poor understood due to their significant complexities and strong heterogeneities, causing challenges for the exploitation and development of these carbonate reservoirs. To better comprehend the heterogeneity of petrophysical and elastic properties of the fault-controlled carbonate rocks, a small carbonate strike slip fault zone is selected, which is located in Yangjikan section in the Tarim basin. We combine the geostatistical, microscopic observation, petrophysical and ultrasonic analyses to characterize and understand the complexities and heterogeneity of petrophysical and elastic properties with different distance to the main fault core. The results show significant complexities and heterogeneities of petrophysical and elastic properties, and the variations of rocks drilled from the fault core are relatively drastic compared to those from the damage zone. The equivalent pore aspect ratios of the rocks are calculated from the differential effective medium theory, the values in the fault core are much higher compared to those from the damage zone, which can discriminate the pore network architectures and can represent reference for determination of the boundary of fractured damage zone. The controlling factors on the heterogeneity of the petrophysical and elastic properties for the selected fault zone are discussed, which mainly include the influence of fault structure position on fracture development, fluid selective filling on effective fracture and pore development, and the sequence on pore development. The results can contribute to the recognition and prediction of the petrophysical and elastic properties and hydrocarbon exploration in carbonate strike-slip fault zone in the Tarim Basin, and can provide reference for the construction of integrate multiscale heterogeneities models.

1. Introduction

The carbonate strike-slip fault reservoirs have become a hot spot for oil and gas exploration, and many associated exploration discoveries have been achieved in Tarim basin in recent ten years (Wang et al., 2020; Qi, 2021; Ma et al., 2022). The faults have a complicated structure, which mainly includes: 1) a single or multiple core zone which contain most of the fault throw; 2) a fractured damage zone; 3) the host rock, also called the protolith. (Mitchell and Faulkner, 2009; Jeanne et al., 2012a). The boundary between the fault core zone and fractured damage zone generally can be determined by the decrease of the fracture or deformation band density, the fault slip and lithology (Wu et al., 2019). However, it is still difficult to accurately describe the boundary of fractured damage zone due to the limited datasets, the heterogeneities and complexities of fault zone (Choi et al., 2016; O'Hara et al., 2017; Wu et al., 2019). The fault zone is formed by fault activity and fluid dissolution transformation (Méndez et al., 2020; Qi, 2021; Wei et al., 2021), and such intense diagenetic process can alter the mineralogy and the structure of the original rocks, causing significant heterogeneities and complexities in rock properties (Tian et al., 2019; Wang et al., 2020), and leading to uncertainties in optimizing well location these carbonate fractured reservoirs.

The fault zones can act as both hydraulic seal and conduit (Pan et al., Wang et al., 2021), hence, it is necessary to understand the petrophysical and elastic properties of these carbonate rocks. The petrophysical and elastic properties of carbonate reservoirs are controlled by porosity, pore

* Corresponding author.
E-mail addresses: cupgongfei@163.com (F. Gong), lbzeng@sina.com (L. Zeng).

https://doi.org/10.1016/j.petrol.2022.111170
Received 22 January 2022; Received in revised form 25 August 2022; Accepted 26 October 2022
Available online 5 November 2022

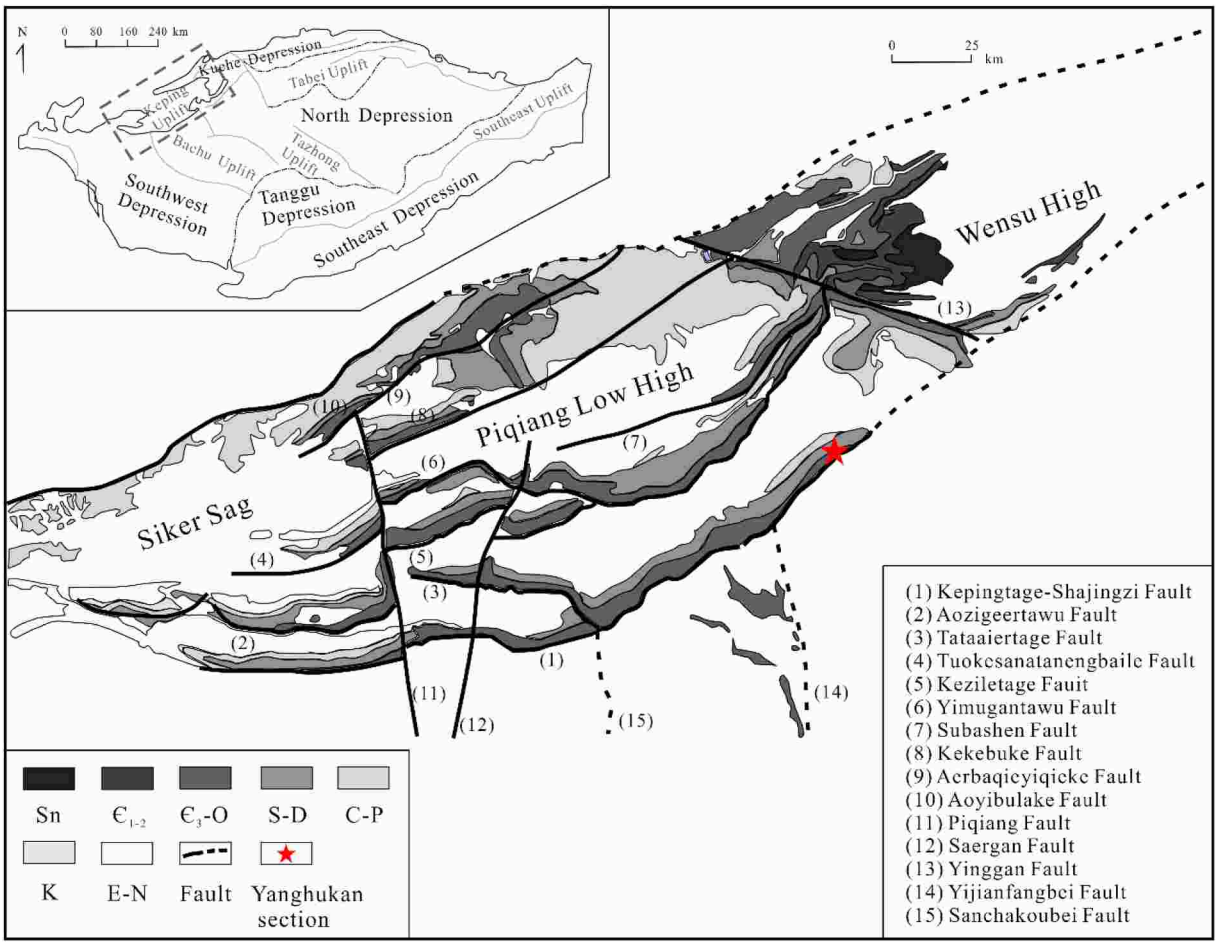

Fig. 1. Division scheme of structural units in Tarim Basin (Modified from Zhou and Du, 2019).

structure and sedimentary environment (Bossennec et al., 2018; Ferraro et al., 2020), which have the complex pore network architectures caused by the sedimentary environments and the complicated diagenetic processes (Zhao et al., 2014). The pore type of carbonate rocks mainly includes interparticle pore, intercrystal pore, moldic pore, intraframe pore, micro-fracture and vuggy (Kenter et al., 2007; Pan et al., 2019; Zhao et al., 2020; Leonide et al., 2012), and these complex pore network architectures cause difficulties to comprehend the petrophysical and elastic properties of carbonate reservoirs. Another challenge for understanding the fault-controlled reservoir properties is the heterogeneity, which exists at all scales and cannot be studied visually during laboratory measurements (Leonide et al., 2012; Zhao et al., 2014; Manoorkar et al., 2021). Previous studies mainly focus on the architectural characteristics, structural evolution and fracture characteristics of the carbonate fault-controlled reservoirs from a geological point of view (Mitchell and Faulkner, 2009; Duan et al., 2020; Xu et al., 2021). Although some researchers studied the porosity and permeability heterogeneity evaluation by rocks drilled from different distance to the main fault core, there is still poor understanding on the permeability with the distance to the main fault core owing to the sparse permeability data (Agosta et al., 2007; Jeanne et al., 2012b; Torabi et al., 2018; Wu et al., 2020). Further, fewer studies have investigated the elastic properties of carbonate rocks controlled by strike-slip fault (Jeanne et al., 2012b; Matonti et al., 2012; Bossennec et al., 2018; Ferraro et al., 2020). Therefore, we are still far from fully comprehending the petrophysical and elastic properties for these carbonate fault-controlled reservoirs, despite being critical to exploration and development.

In this study, a small carbonate strike-slip fault zone is selected to investigate the petrophysical and elastic properties of carbonate rocks, which is located in Yangjikan section in the Tarim basin, China. Firstly, we combine the geostatistical, microscopic observation, petrophysical and ultrasonic analyses on outcrops drilled from different distance to the fault core to characterize and understand the heterogeneity of petrophysical and elastic properties. Secondly, the equivalent pore aspect ratios are calculated to discriminate the pore network architectures based on differential effective medium (DEM) model. Finally, the controlling factors on heterogeneity of the petrophysical and elastic properties from fault zones growth are discussed.

2. Geological setting

The studied carbonate strike-slip fault zone is located in Yangjikan section in the Tarim basin, China, whose geographical coordinate is (N40° 25′ 29.27″, E79° 10′ 15.6″), with an overall strike of nearly north-south and a total length of about 900 m–1000 m. The Yangjikan section located in the south of Keping tectonic unit on the northwest edge of Tarim Basin (Fig. 1), and the Keping tectonic unit experienced multi-stage tectonic movements such as Caledonian, Hercynian and

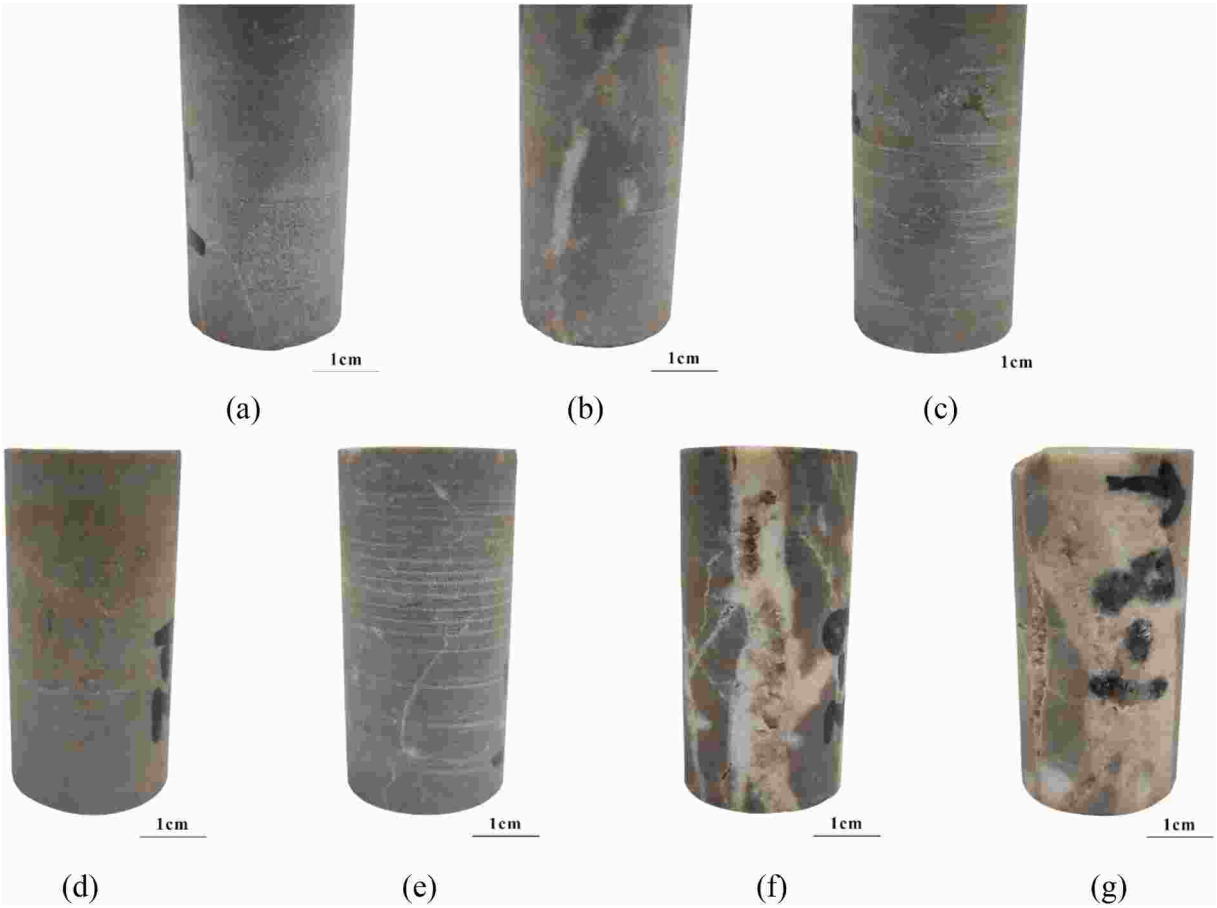

Fig. 2. The core samples drilled from different distance to the main fault core. (a) 5.04 m, (b) 4.6 m, (c) 2.6 m, (d) 1.5 m, (e) 1 m, (f) 0.1 m to the fault core. (g) Samples drilled from the fault core.

Himalayan period (Zhou and Du, 2019). In the Cenozoic, multi-stage tectonic faults and nappes were formed in Keping tectonic unit which was affected by the remote effect of Eurasian plate collision and the revival of the South Tianshan orogenic belt, and the near east-to-west and the near north-to-south trending faults are mainly developed in this unit (Zhou and Du, 2019). The Yingshan formation of middle and lower Ordovician is mainly exposed in Yangjikan section, which is mainly comprised of two parts from top to bottom: the lithology of the lower part is dominated by gray-white, dark gray medium thick algal debris cohesive limestone mixed with mud-bright crystal sand debris, micrite limestone and gray medium-silty dolomite, the geological age is Daobaowan period of Early Ordovician. The lithology of the upper part is dominated by light-dark gray medium-thick micrite limestone, laminated micrite limestone and medium-thick micrite-bright arenaceous limestone interbedded, with a small amount of flint bands inside, the geological age is Dawan period of Middle Ordovician (Wang et al., 2019).

3. Samples and methods

The outcrops are conducive to comprehend the fault-zone architecture, distribution and types of carbonate rocks controlled by strike-slip fault, which are helpful to study fluid flow and can be used for our measurements (Mercuri et al., 2020; Geng et al., 2021). The studied carbonate outcrops are drilled from different distance to the fault core from a strike-slip fault zone from Yangjikan section in the Tarim basin. Note that the rock properties of outcrops slightly differ from those of the subsurface due to the long-term weathering, and hence the weathered layers should be cut before preparing the cylindrical specimens. To meet the requirement of measurements, the cylindrical core samples with different distance to the main fault core are prepared with a diameter of 25 mm, height about 50 mm as shown in Fig. 2, and two core samples are drilled from each outcrop to increase the credibility of the measured data. It can be observed that the cores have little visible porosity due to they are extremely dense, and a few dissolution vugs can be observed in core samples drilled from the fault core (Fig. 2). The leftover sample from cutting is used for whole-rock mineral analysis, scanning electron microscopy (SEM) and optical thin-section analysis to characterize the micro-textures, pore and diagenetic features of these carbonate rocks. The porosity and permeability of cores are respectively measured by using the HPP100 instrument with nitrogen as the reference fluid at ambient conditions, and the permeability is obtained by Pulse-Decay technique (Petunin et al., 2011). The ultrasonic velocities of dry core samples are measured using ultrasonic pulse test system at room temperature and atmospheric pressure, and the dominant frequency of ultrasonic transducer is 0.5 MHz.

4. Results and analysis

4.1. Macro-fracture features

The overall trending of the studied carbonate strike-slip fault zone is nearly NNW, and the structure of the fault zone is divided according to the position of the boundary sliding surface, as shown in Fig. 3. A narrow

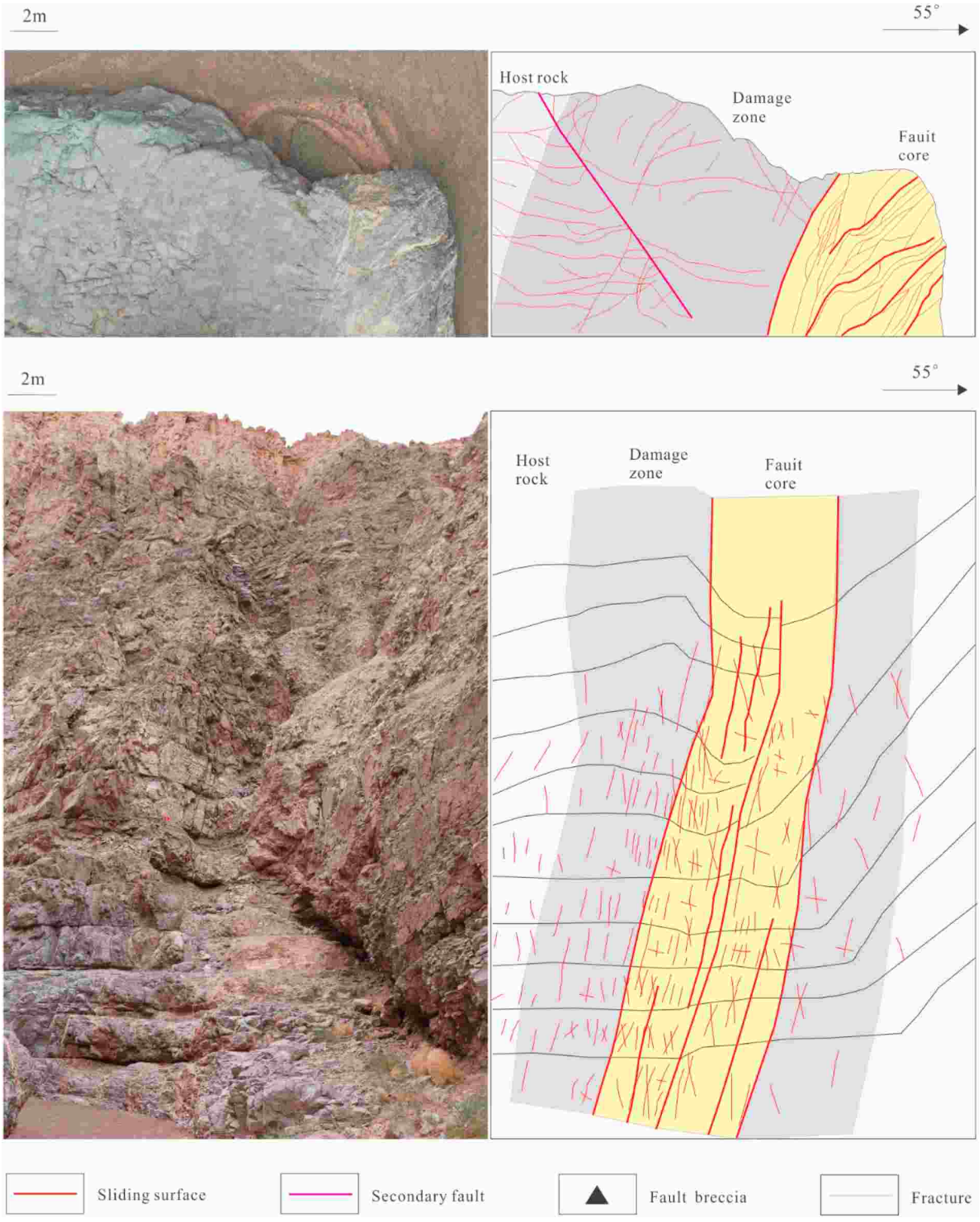

Fig. 3. Satellite map and outcrop photos of the studied strike-slip fault.

main fault core with 1 m–2 m wide can be found, and the rocks in the fault core are strongly broken. Multiple sets of sliding surfaces can be observed, which are completely filled by calcite veins, with a width of 10–20 cm. There are fracture damage zones on both sides of main fault core with an extension range of about 4–7 m. Note that three groups of fractures with different occurrences are mainly developed in the damage zone: the first group of fractures has an inclination of about 80°, the second group of fractures is nearly horizontal, and the third group of fractures is parallel to the sliding surface. Note there is an associated secondary fault at 4.6 m away from the east of the main fault core, and the influence should be discussed in later.

The fractures in the fault zone are generally generated by multiple fault activity, which can control the development of reservoir space and provide the pathways for hydrocarbons flow (Wang et al., 2020; Qi, 2021). Hence, the fracture features at the outcrop scale are investigated and shown in Fig. 4. The linear density and the spacing of fractures are shown in Fig. 4a–(b), the fractures are most developed at the fault core, with a linear density of 40 fractures per meter and a minimum spacing of

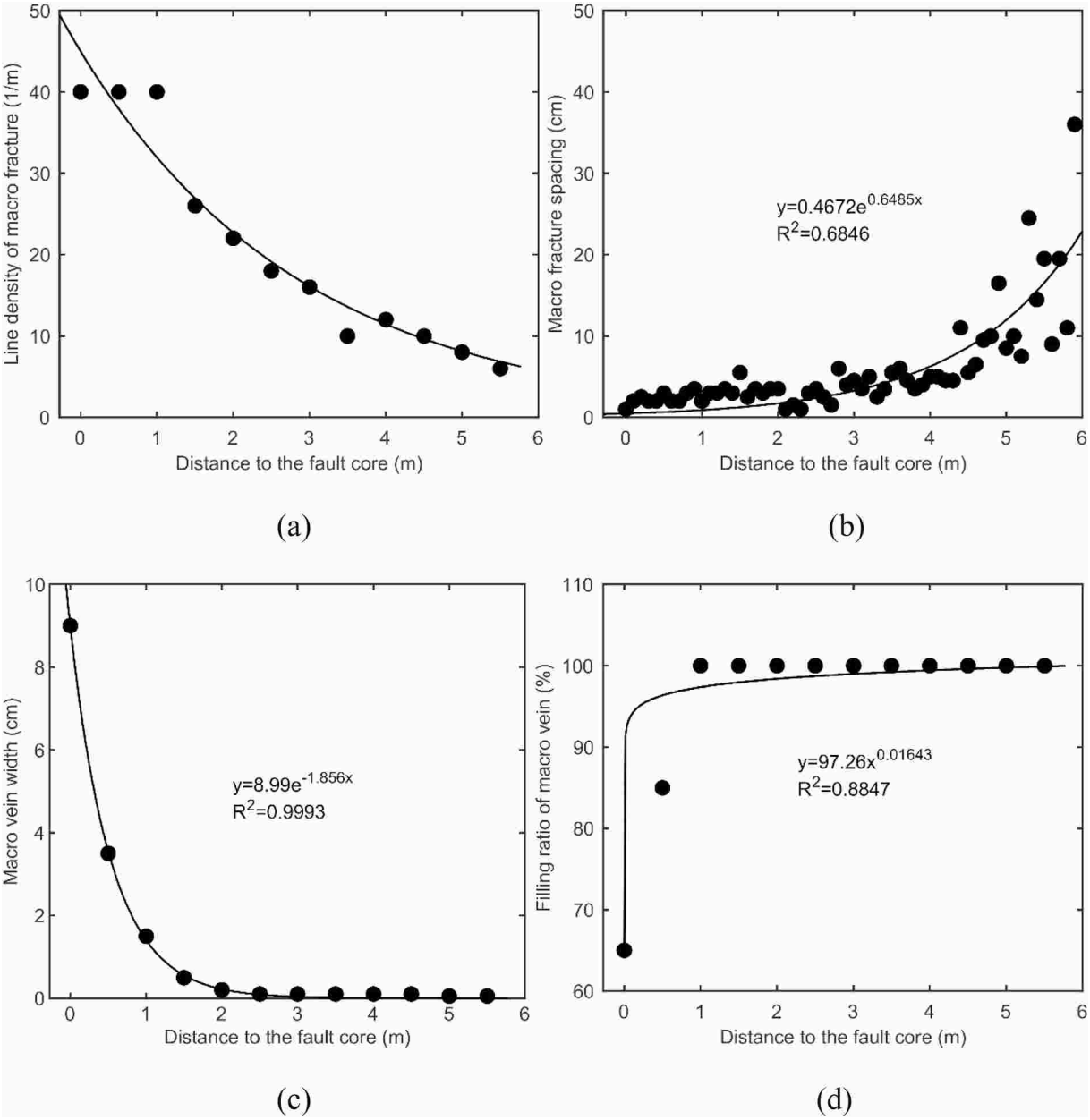

Fig. 4. The macro-fractures feature in different areas of the fault zone. (a) Line density of macro fracture, (b) Spacing of Macro fracture, (c) Width of macro vein, (d) ratio of macro vein.

1 m. The linear density of fractures decreases and the fracture spacing increases with the distance to the main fault core. Fig. 2 shows that the fractures in studied core samples are filled with calcite veins with different levels, thus the width and the degree of filling are also investigated as shown in Fig. 4c–(d). In the fault core, the fractures are mainly fully filled or semi filled with calcite vein, but they are mainly fully filled with calcite vein in the damage zone, and the filling degree of calcite vein increases with the distance to the main fault core. The width of calcite vein in the fault core is the largest, which can reach 8–10 cm, and gradually decreases to both sides from the main fault core. In the area about 2 m to the fault core, the filling width has been reduced to about 0.3 cm, which is difficult to distinguish.

4.2. *Micro-structural analysis*

4.2.1. *Pore type and structure*

The Yangjikan section mainly exposes the Ordovician Yingshan formation carbonate rock stratum and subject to complex diagenesis in the long geological history, causing the original pores are difficult to preserve, thereby, which mainly develops secondary pores mainly including the dissolution pores, vugs and fractures (Zhao et al., 2016; Pan et al., 2015; Ferraro et al., 2020). Figs. 5 and 6 show the thin sections for the sample from the fault core and the damage zone with 5.04 m to the fault core, respectively. According to the thin section observations, multiple dissolution pores in the rock are occurred along the

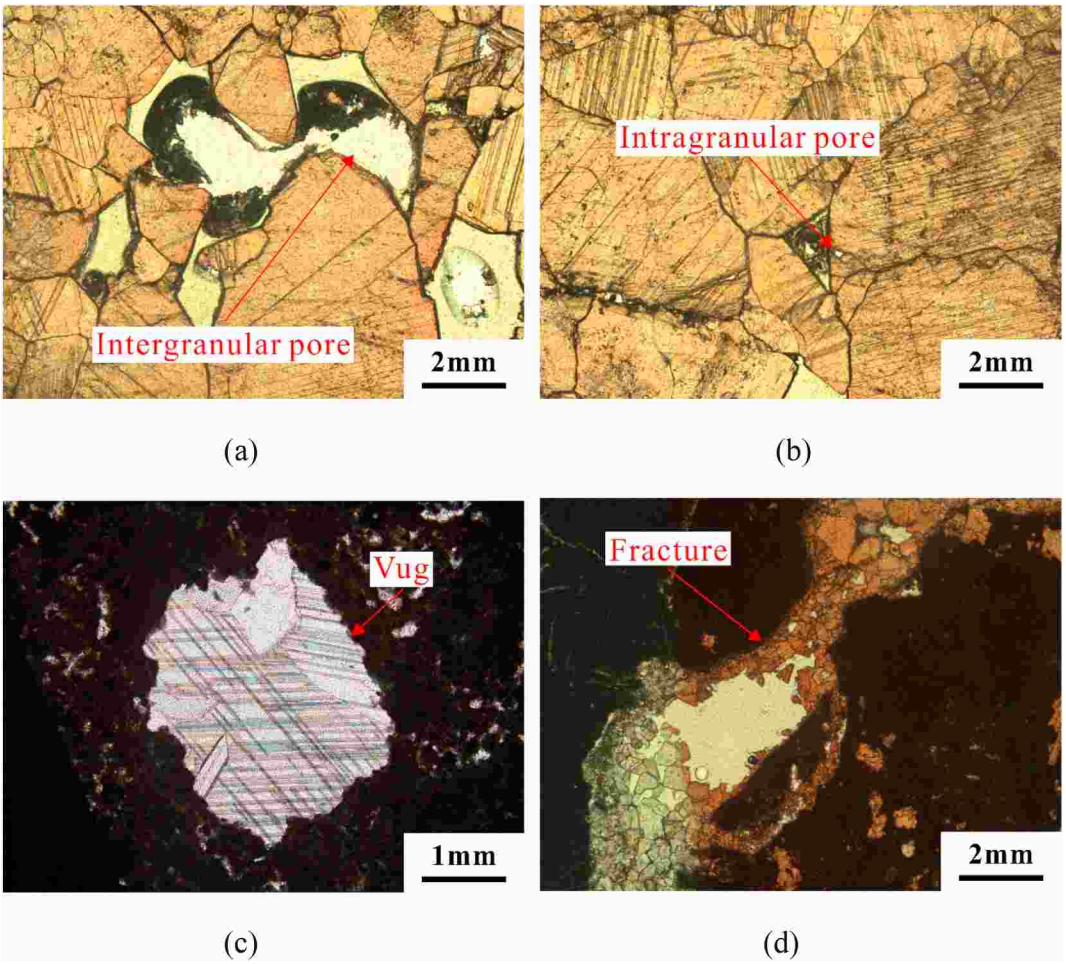

Fig. 5. Thin sections photomicrographs showing main pore types of the samples from the fault core. (a) Intergranular pore. (b) Intragranular pore. (c) Vug. (d) Fracture.

fractures, and most of them are filled with calcite crystal due to the strong fluid filling in the later diagenesis stage, these phenomena also can be observed in the core samples (Fig. 2). Based on the pore classification (Choquette and Pray, 1970; Lønøy, 2006), four pore types are classified based on the thin section observations, mainly including dissolved intergranular pores (Figs. 5a and 6a), intragranular pores (Fig. 5b), vugs (Figs. 5c and 6b) and fractures (Figs. 5d and 6c). Intergranular pores refer to the chamber between fine-grain with the size is about 0.2 – 2 mm (Figs. 5a and 6a), which are mainly formed in the space that are not occupied by calcite cement and the space after coarse-grained calcite residue or local dissolution in microcracks. Intragranular pores are tiny pores on the crystal surface of minerals, which are mostly circular or oblate. The range of intragranular pores observed in the studied rock is 0.5–1 μm (Fig. 5b). The intergranular and intragranular pores are poorly developed in these studied rocks, both of them can be observed in the fault core (Fig. 5a and b), while the intergranular pores only can be observed in the damage zone (Fig. 6a). Vugs are defined as the pore size more than 2 mm formed by dissolution mechanism and often associated with fractures, and they are widely developed in the studied rocks, however, almost all vugs are fully filled with calcite crystals, and the residual space is less than 10%. The diameter of the vugs in the fault core is about 3–4 mm (Fig. 5c), while that in the damage zone is about 2–2.5 mm (Fig. 6b). The Fractures or microfractures are widely developed in the studied rocks (Figs. 5d and 6c), which should be formed by tectonic stress release. The extension of width for fractures or microfractures vary greatly in the fault core, the width of microfractures range from 1 mm to 5 mm (Fig. 5d), while the width is only less than 0.5 mm in the damage zone (Fig. 6c). Almost all fractures and micro-fractures are filled or semi filled with coarse-grained calcite (Figs. 5d and 6c), causing the poor connectivity of these carbonate rocks.

4.2.2. *Micro-fracture features*

For micro-fractures in carbonate reservoirs, which generally refer to fracture opening less than 0.5 mm, and they also have storage and transport capacity (Zeng et al., 2010; Guo et al., 2020). Thus, the fracture features on the micro-scale are characterized by the thin sections and SEM observation. For the fault core samples, the fracture width mainly ranges from 1 mm to 5 mm, and the minimum width is less than 0.5 mm based on the thin sections and SEM observation. Fig. 7a shows multiple groups of fractures are developed in the fault core samples, and there is a widest main fracture with a width of 6 mm in the center of the field of view which almost fully filled with calcite crystals, and a large number of micro-fractures and small filled vugs are distributed around

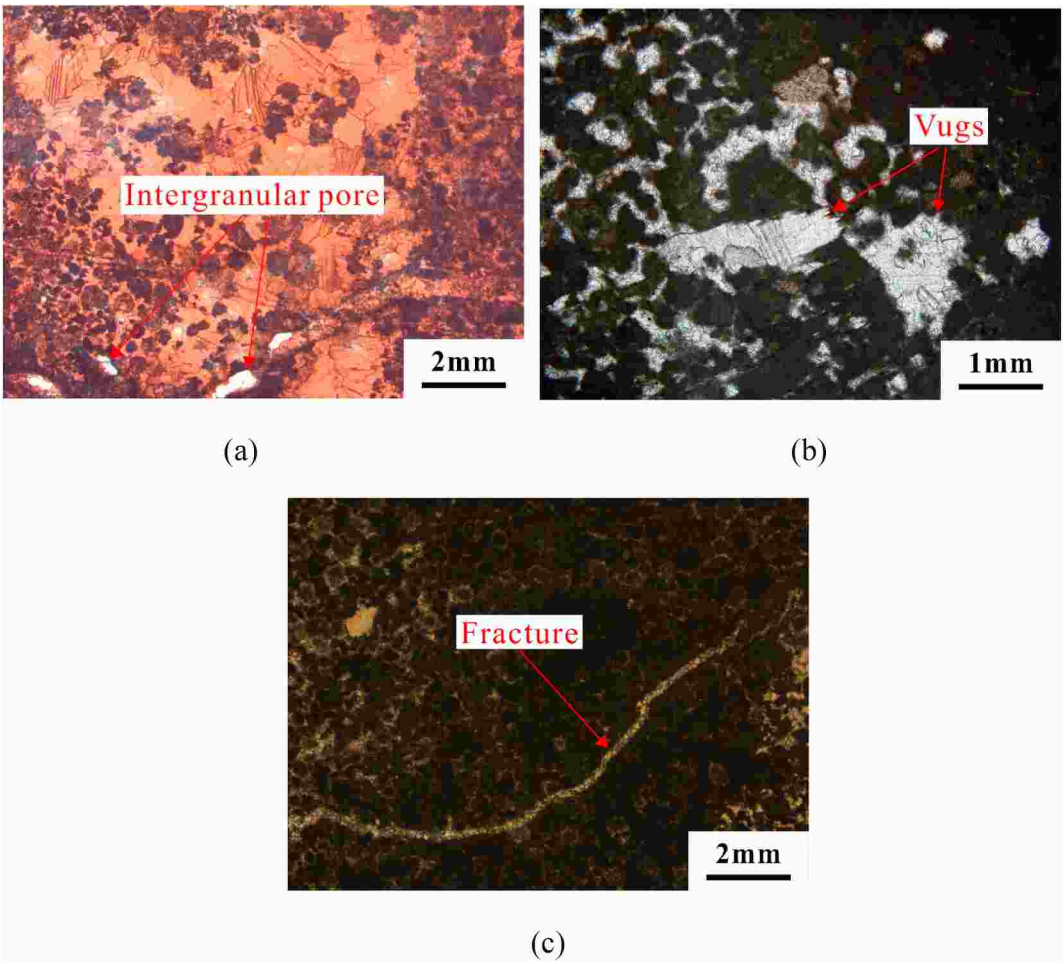

Fig. 6. Thin sections photomicrographs showing main pore types of the samples from the damage zone with 5.04 m to the fault core. (a) Intergranular. (b) Vug. (c) Fracture.

it. Fig. 7b shows that an obvious micro-fracture with a fractured opening of about 10 μm and length of about 0.5 mm–0.7 mm can be observed based on the SEM picture, and the visible part in the micro-fractures is filled with calcite crystals. For the damage rock from 5 m to the fault core, only one microfracture with long extension can be observed based on the thin section which the width is less than 0.5 mm, and the interior is fully filled with calcite crystals as shown in Fig. 7c. The rock is extremely dense and it is difficult to identify microfractures from the observation of SEM pictures, only one suspected micro-fracture with a width of about 8 μm can be observed on the surface of mineral grain as shown in Fig. 6d.

The density, filling width and filling ratio of calcite veins of fractures and microfractures are counted by microscopic statistical method (Fig. 8), and these microfracture fractures are consistent with the macro-fractures features at the outcrop scale. Fig. 8a shows that the density of microfractures decreases with the distance to the main fault core. The filling width of micro veins decreases while the filling ratio of micro veins increases with the distance to the main fault core (Fig. 8b and c). The microfractures in the fault core are mainly semi or fully filled, while they are all fully filled in the damage zone, which should be related to the fluid flow resistance caused by hydrodynamic paths with different widths in these two regions.

4.3. Porosity and permeability variations

The porosity, permeability and other basic parameters of studied core samples are shown in Table 1. Fig. 9 shows that the porosity and permeability of core samples, which display wide variations, suggesting a strong heterogeneity in petrophysical properties. The porosities of the samples drilled from the fault core are 6–7 times larger than those drilled from the damage zone, and the permeabilities of the samples drilled from the fault core are much higher than those from the damage zone by 3–4 orders of magnitude. Note that there is obvious difference in porosity and permeability values measured from two cores drilled from the same outcrop, especially for rocks from the fault core, which further suggests the strong heterogeneity of the petrophysical properties in these carbonate rocks. The variations of porosity and permeability of samples from the fault core are relatively drastic compared to those from the damage zone, the overall variation of porosity and permeability is relatively stable in the damage zone. The scattering can be observed in cores from 4.6 m to the main fault core owing to the presence of secondary faults in this position. These petrophysical properties are consistent with the fracture features discussed in Figs. 3 and 8. Based on the thin sections and SEM observation, a large number of fractures are almost completely filled with calcite veins in the damage zone, although

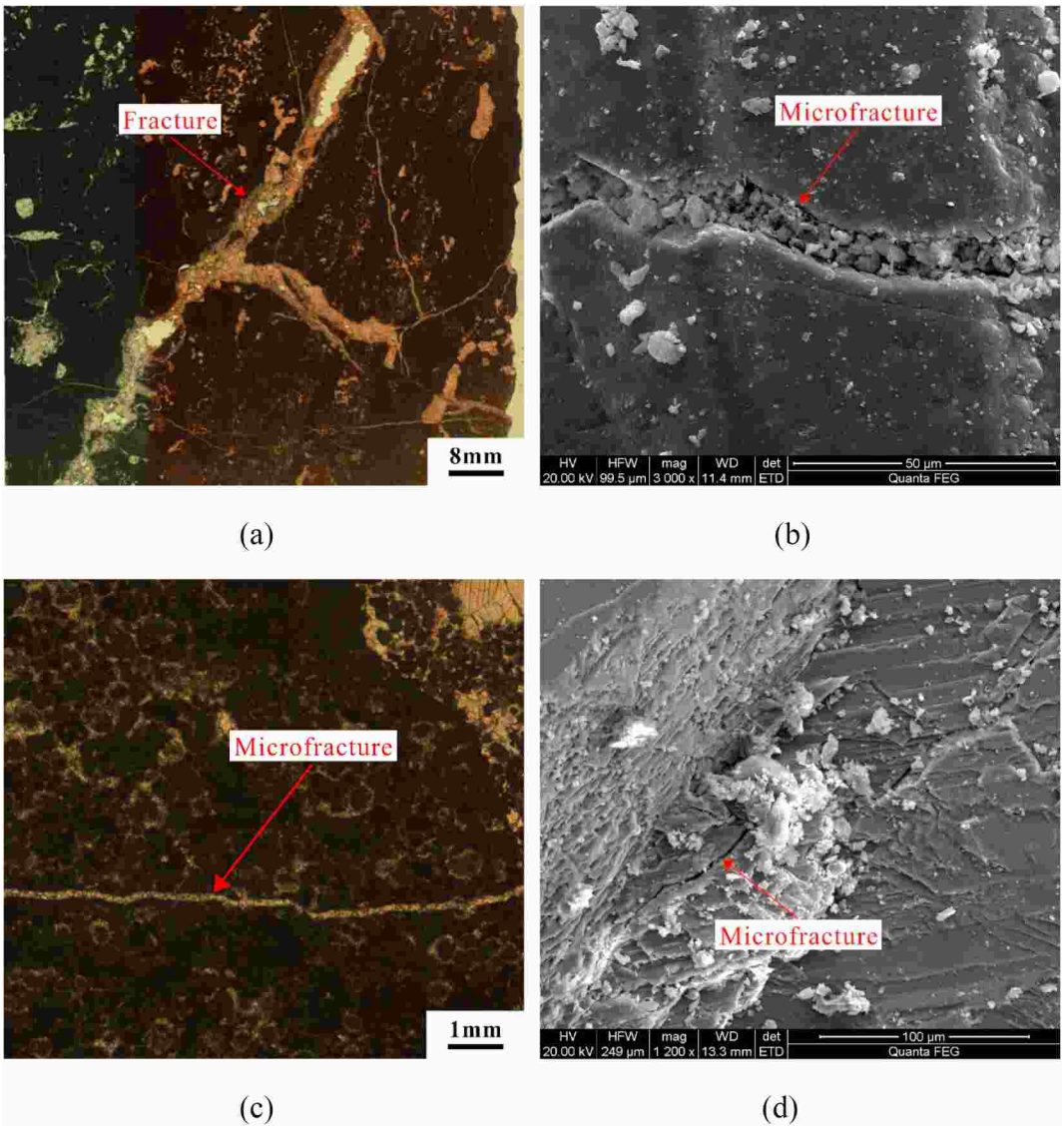

Fig. 7. The thin sections and SEM pictures showing fractures and microfractures of carbonate samples from the fault core and fracture damage zone. (a)–(b) Samples from the fault core; (c)–(d) samples from the damage zone, 5.04 m from the fault core.

centimeter level small vugs are developed, they are filled with calcite crystals and cannot connect with each other, causing the reduction in porosity and permeability. The key factors affecting the heterogeneity petrophysical properties will be discussed later.

Fig. 10 shows the correlation between the porosity and permeability, a good positive correlation between them can be observed in whole range of carbonate fault zone. However, the correlation is different in these two regions, the slope in the fault core is much larger than that in the damage zone due to the strong tectonic action and fluid activities. These behaviors suggest that tectonic faulting in the fault core can greatly improve the physical properties of the reservoir, especially for the permeability, which are conducive to the formation of oil and gas storage space and migration channel.

4.4. Elastic properties variations

Fig. 11 shows that the velocities of the rocks from the damage zone are much higher than those from the fault core, which are consistent with previous studies (Jeanne et al., 2012a, 2012b; Torabi et al., 2018; Ferraro et al., 2020). The values for the P-wave velocity in the fault core can be as low as 4198 m/s, and gradually increases to the surrounding, and can be as high as 6078 m/s in the damage zone, suggesting the strong heterogeneity of elastic properties within a few meters. There is obvious difference in values measured from two cores drilled from the same outcrop, especially for cores from the fault core, which further suggests the strong heterogeneity of the elastic properties in carbonate rocks controlled by strike-slip fault. Compared to the P-wave velocity, the S- wave velocity is more sensitive to the distance to the fault core. Detailly, with the distance range from 0 m to 5.04 m to the fault core, the P-wave velocity increases 44.8% from 4198 m/s to 6078 m/s, while S-wave velocity increases 52.8% from 1957 m/s to 2992 m/s. Note that there is a slight drop at about 4.6 m to the fault core, which is caused by the development of secondary faults. The velocities show strong heterogeneity in different areas of carbonate fault zone, and the main factors are porosity, pore structure and sedimentary environment (Bossennec et al., 2018; Ferraro et al., 2020).

The correlation between the velocities and petrophysical properties (porosity and permeability) are shown in Fig. 12. The velocities decrease with the increase of porosity and permeability, which agree well with previous experimental and theoretical results (Berg et al., 2017; Abdlmutalib et al., 2019; Garia et al., 2021). Note that both P- and S-wave velocity exhibit a rapid decrease in the fault core, and a gentle decrease

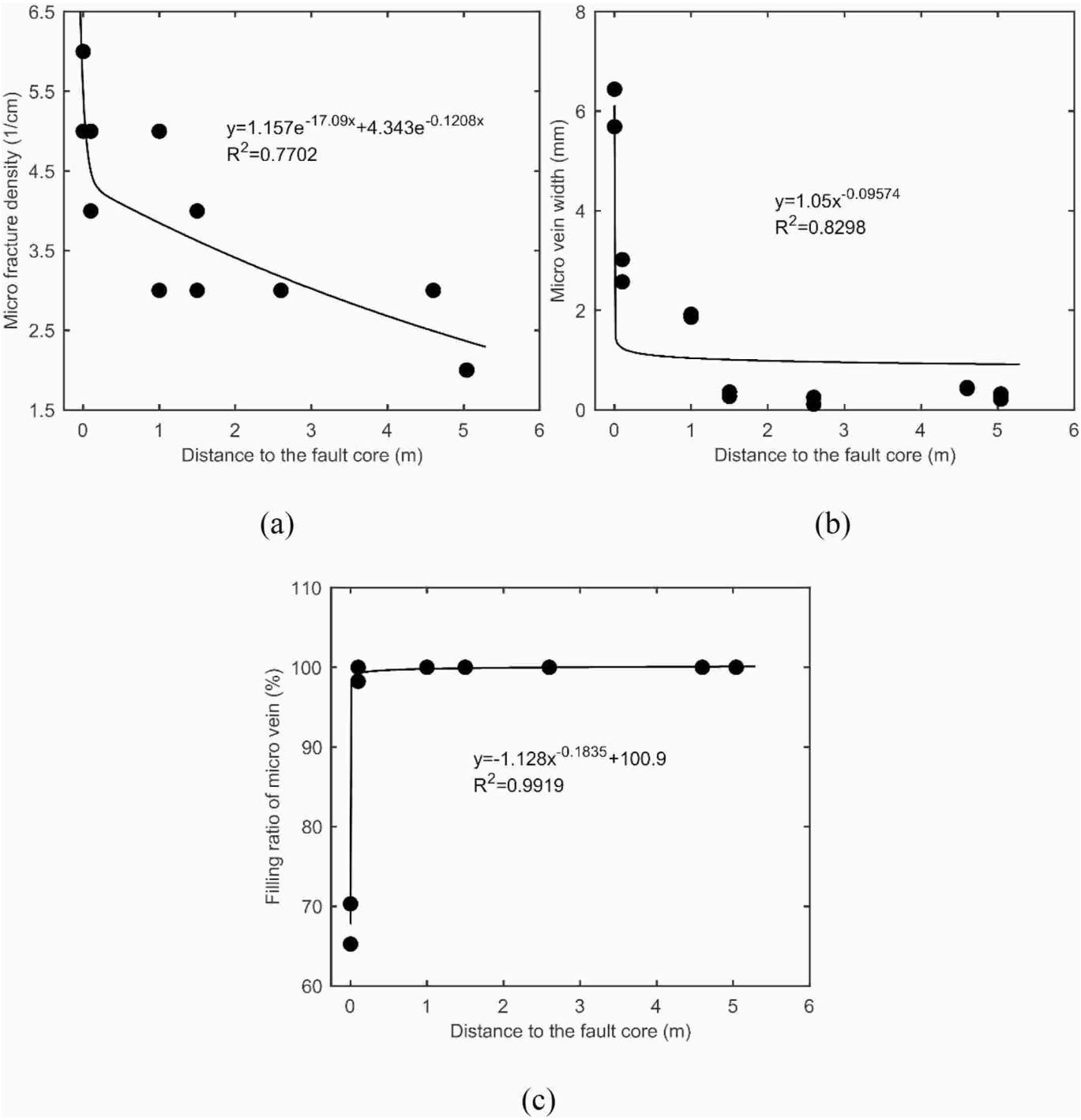

Fig. 8. The macro-fractures feature in different areas of the fault zone. (a) Density of microfractures, (b) Filling width of micro veins, (c) Filling ratio of micro veins.

in the damage zone, indicating the control difference of reservoir properties caused by the structural of fault. The characteristics in these relations can be used for qualitative identification for the fault core and the damage zone.

4.5. Equivalent pore aspect ratios of carbonate rocks

For a given porosity, the elastic properties of carbonate rocks generally exhibit a wide scattering with the same mineral composition due to the complicated pore structure (Verwer et al., 2008; Pan et al., 2019). The accurate prediction of the pore network architectures of carbonate fault zone is extremely difficult due to the complex diagenetic process and sedimentary environment. To quantitatively characterize the pore network architectures of carbonate fault zone, the geophysical pore type named equivalent pore aspect ratio is discussed in this paper, which can derive from some effective medium theories such as self-consistent, DEM, and KT model (Kuster and Toksoz, 1974; Norris, 1985; Mavko et al., 2003). The results derived from these effective medium theories have been proven to only exhibit very small differences, but the DEM and KT models are more suitable to use for carbonate rocks comprising large amounts secondary pores (Wang et al., 2015; Fournier et al., 2011, 2018). Thus, the DEM theory is selected to derive the average aspect ratios, and the expression of DEM model are as follows:

Table 1
The basic parameters of the selected carbonate rocks.

Samples	Density (g/cm^3)	Porosity (%)	Permeability (mD)	Calcite (wt%)	Quartz (wt%)
Carb-0-1	2.68	5.37	7.6592	97.7	2.3
Carb-0-2	2.65	5.31	4.9944	99.1	0.9
Carb-0.1-1	2.58	5.16	2.6525	98.7	1.3
Carb-0.1-2	2.57	5.25	3.5369	98.2	1.8
Carb-1-1	2.69	0.45	0.0048	97.9	2.1
Carb-1-2	2.67	0.5	0.0055	98.6	1.4
Carb-1.5-1	2.71	0..51	0.0091	97.6	2.4
Carb-1.5-2	2.7	0.62	0.0121	99.4	0.6
Carb-2.6-1	2.69	0.52	0.0061	99.8	0.2
Carb-2.6-2	2.7	0.4	0.0036	99.1.	0.9
Carb-4.6-1	2.67	0.94	0.0152	97.5	2.5
Carb-4.6-1	2.67	0.91	0.0091	98.8	1.2
Carb-5.04-1	2.68	0.5	0.0034	98.4	1.6
Carb-5.04-2	2.69	0.51	0.005	99.2	0.8

$$(1-y)\frac{d}{dy}[K^*(y)] = (K_2 - K^*)P^{(*2)}(y) \quad (1)$$

$$(1-y)\frac{d}{dy}[\mu^*(y)] = (\mu_2 - \mu^*)Q^{(*2)}(y) \quad (2)$$

where φ represents the rock porosity; K_2 represents the bulk modulus of the pore fluid; K^* and μ^* are the effective bulk and shear modulus of the dry rock, which can be predicted the knowledge of the elastic modulus of the minerals, the porosity and the weight fraction of each mineral listed in Table 1. $P^{(*2)}$ and $Q^{(*2)}$ are polarization factors as functions of α_K and α_μ, respectively (Mavko et al., 2003).

By assuming the shape of the pores is ellipsoid, the equivalent pore aspect ratio can be defined as the ratio of the polar to equatorial lengths. The equivalent pore aspect ratio includes two parameters, α_K and α_μ, which can be derived by matching the bulk and shear moduli of carbonate rocks from laboratory experimental with theoretical results, respectively (Fournier et al., 2011, 2018; Pan et al., 2019). Although the equivalent pore aspect ratios α_K and α_μ are not the actual geometric pore type, but they can describe the actual pore network architectures to some extent, and which can be considered as parameters illustrating the influence of the pore network architectures on the bulk and shear moduli of carbonate fault zone. The bulk and shear moduli can be calculated from the velocity and the density of the dry carbonate rocks according to Eqs. (3) and (4). Based on the DEM theory, the equivalent pore aspect ratio inversion templates can be established, and the experimental results are also plotted in Fig. 13. The inversion templates can illustrate the influence of porosity and the pore aspect ratio on the elastic properties of carbonate rocks, which decrease with the increase of porosity and increase with the increase of the equivalent pore aspect ratio for a given porosity.

$$K = \rho\left(V_P^2 - \frac{4}{3}V_S^2\right) \quad (3)$$

$$\mu = \rho V_S^2 \quad (4)$$

where ρ is the bulk density of rocks, K and μ is the bulk and shear moduli, V_P and V_S is P- and S-wave velocity of rocks, respectively.

The variations of the equivalent pore aspect ratio, α_K and α_μ, of the samples are shown in Fig. 14a and b, respectively. For the studied

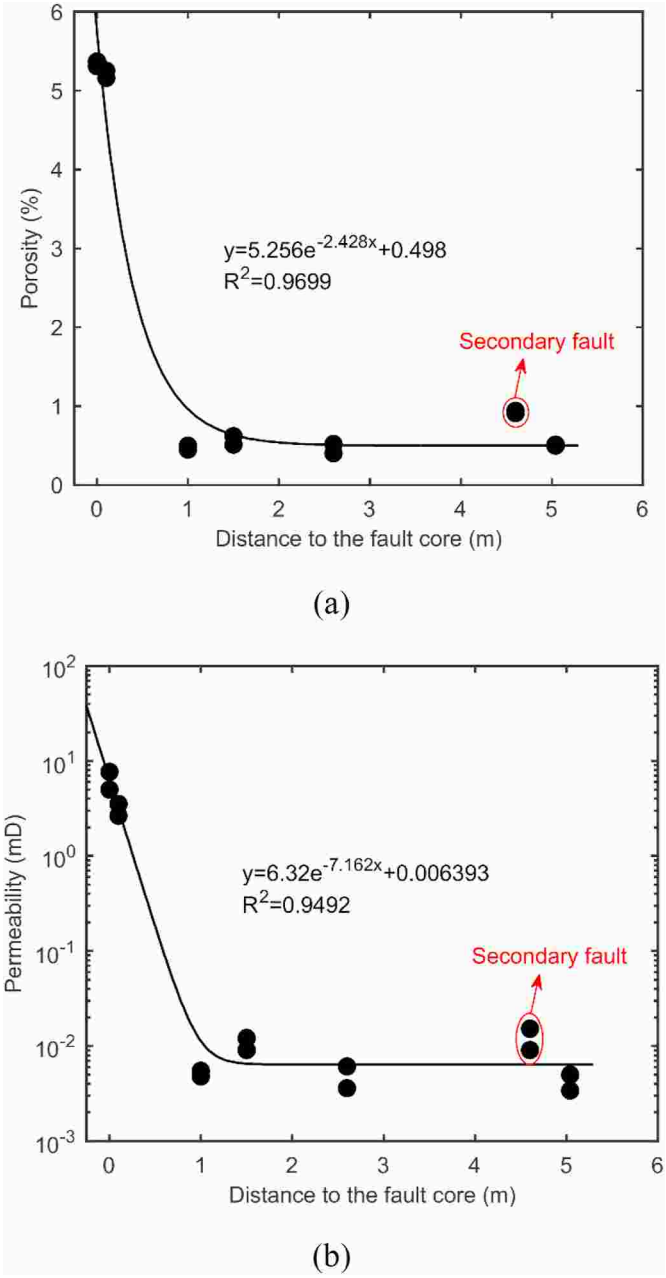

Fig. 9. The Porosity and Permeability variations of the core samples drilled from the different distance to the fault core.

samples, the values of α_K range from 0.0396 to 0.0862, with the average value is 0.0571; the values of α_μ range from 0.0061 to 0.0256, with the average value is 0.0127. The values of α_K are always larger than the values of α_μ of these samples, because these carbonate rocks are mainly developed with secondary dominated by dissolution pores, vugs and microfractures, and this phenomenon has been found in dissolution pore carbonate rocks (Fournier et al., 2018; Pan et al., 2019). Note that the values of equivalent pore aspect ratio in this study is smaller than the previous inversion results from Fournier et al. (2018), which could be attributed to the low porosity of the studied samples (<6%). The value of α_K and α_μ decrease with the distance to the main fault core, which are consistent with the fracture features discussed above. The equivalent pore aspect ratio of the samples in the fault core are much higher than that of the damage rocks, taking the α_K as an example, for the samples drilled from fault core $0.0747 \leq \alpha_K \leq 0.0862$, while $0.0396 \leq \alpha_K \leq 0.0598$ for the samples from the damage zone. This is mainly because the

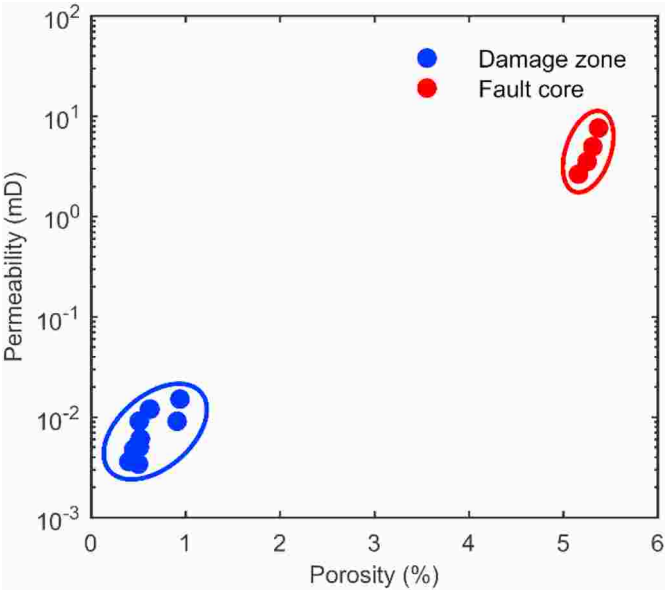

Fig. 10. The correlation between the porosity and permeability of the carbonate rocks controlled by strike-slip fault.

dominant pores in the samples from the fault core are the Vugs and intragranular pores, while the dominant pores in the samples from the damage zone are the small fractures with high filling degree which almost no residual pores are existed. Hence, the equivalent pore aspect ratio can be considered as relevant parameters for distinguishing the pore network architectures in carbonate rocks, such as pore types and diagenetic fabrics, and can provide references for the boundary identification of fractured damage zone.

5. Discussion-key factors controlling heterogeneity of the strike-slip carbonate fault zone

As shown in Figs. 9 and 11, the petrophysical and elastic properties display significant complexities and strong heterogeneities. For example, the variations of petrophysical and elastic properties of samples from the fault core are relatively drastic compared to those from the damage zone, the overall variation of them is relatively stable in the damage zone. Previous studies pointed out that the main factors affecting the heterogeneity of carbonate reservoir include structural faults and fluid activities (Wennberg et al., 2013; Duan et al., 2020; Guo et al., 2020).

For the studied carbonate strike-slip fault zone, the fractures caused by structural faults are the main reservoir space and seepage channel. During the formation and evolution of the fault zone, the different parts of the fault zone experienced great differences in the tectonic stress with magnitude and direction, and the complex effects of fluid activities, causing the difference in development of fractures as shown in Figs. 4 and 8, which reflects the strong heterogeneity of fracture development under the control of different structural parts in the fault zone. The fluid carries a large number of trace mineral components, which can be affected by many factors such as rock properties, external temperature and pressure conditions and fluid mineralization in the process of vertical migration along the main fault, minerals with calcium and other components should be precipitated in fractures or karst caves under supersaturation conditions, causing the pore space formed previously is filled or blocked (Jiu et al., 2020; Couto et al., 2021; W.B Zhang et al., 2021). According to the microscopic observations and the analysis from

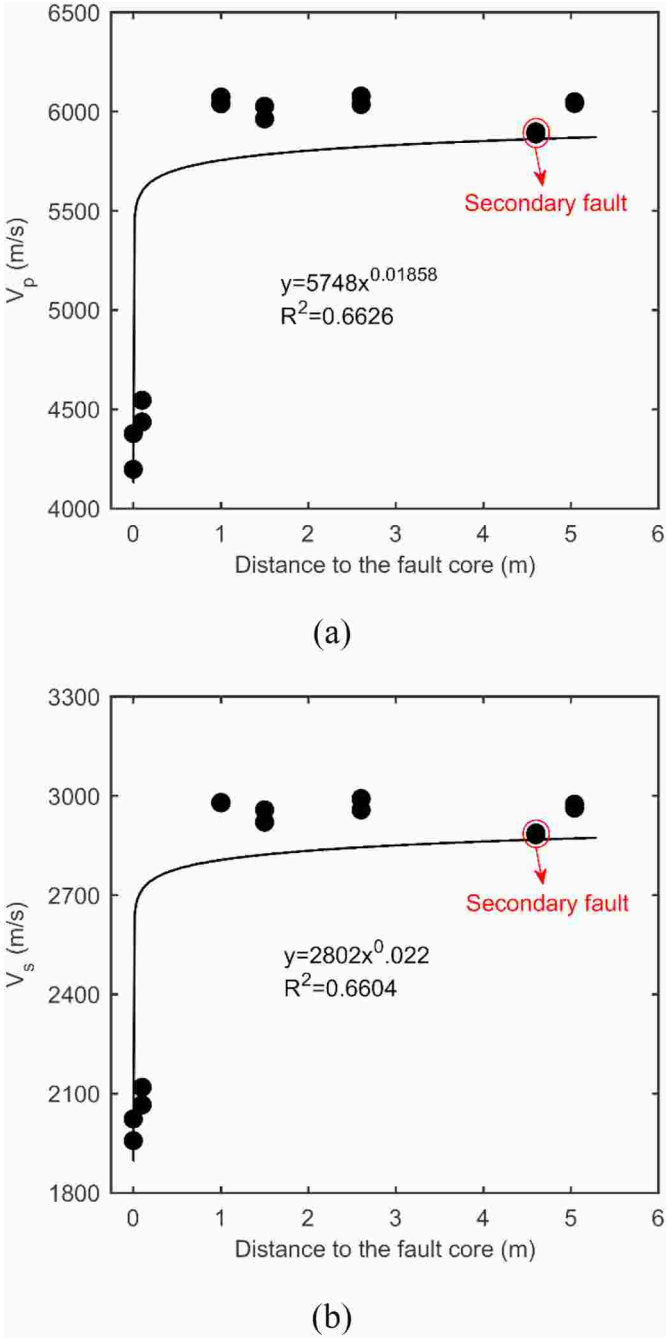

Fig. 11. The P- and S-wave velocities variations of the core samples with the distance to the fault core.

the fracture features discussed above, the developed fractures in the studied carbonate strike-slip fault zone are widely filled with semi in the fault core and are fully filled in the damage zone. This is because most of the fractures in the damage zone mainly experience filling action from the later fluid activity, while the fault core is more strongly affected by structural fault activity than filling action, which retaining a large amount of reservoir space. These difference in the distribution pattern and filling of fractures between the fault core and damage zone should cause strong heterogeneity for the petrophysical and elastic properties of the studied carbonate strike-slip fault zone.

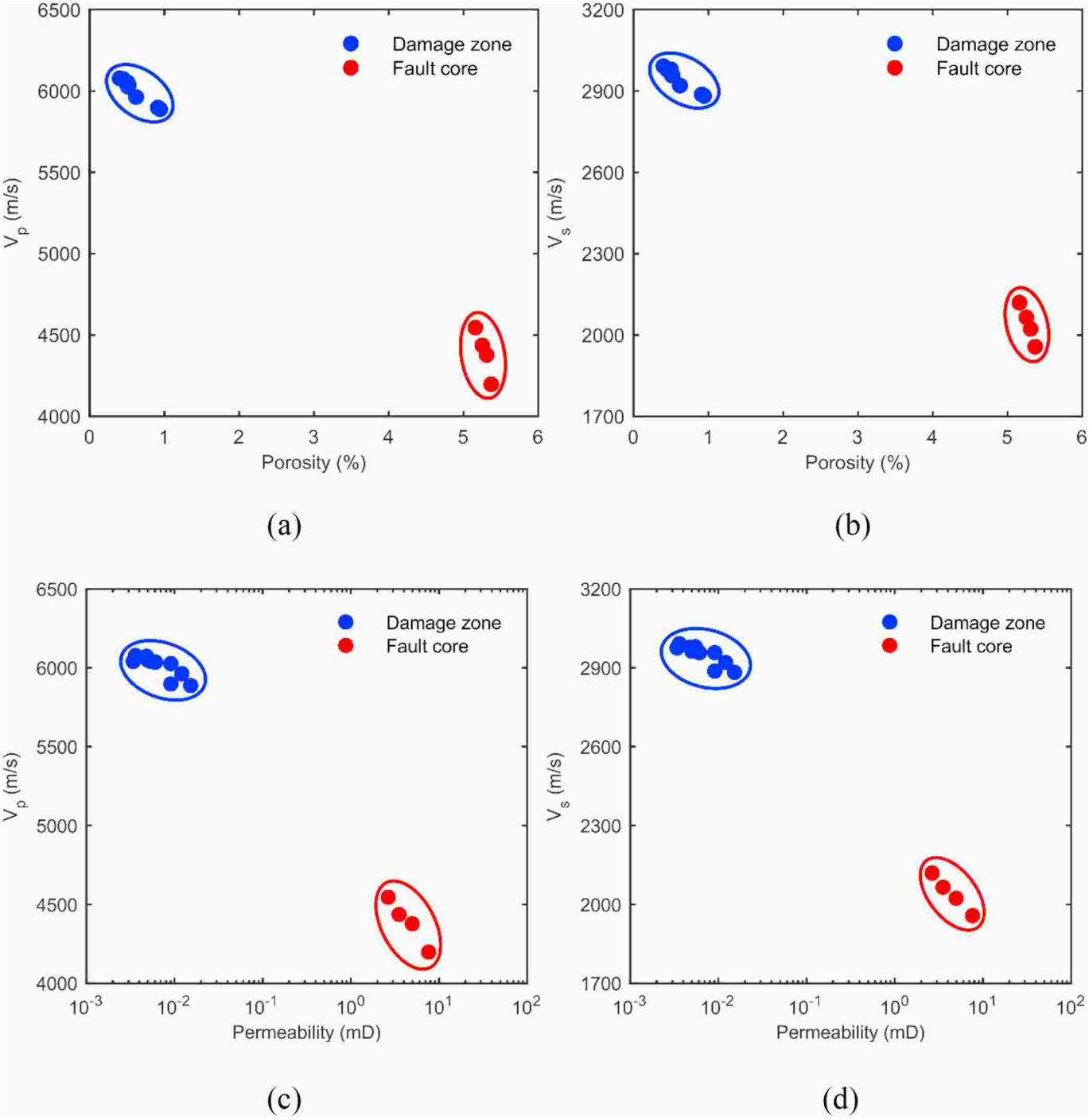

Fig. 12. The correlation between the velocities and petrophysical properties (porosity and permeability) of the carbonate rocks controlled by strike-slip fault.

The main fault core is the main object of fluid dissolution as the channel of vertical fluid migration, and the fluid mainly migrates along the interconnected sliding surface, the gap between fractures and fault breccia in the main fault; while the connected fractures are the main migration channel in the damage fracture zone (Smeraglia et al., 2021). Due to the strong tectonism, the main fault can produce large voids which is easier to form the dominant migration channel of fluid, and it is also the area where fluid dissolution is most likely to occur (Michie and Haines, 2016; Wu et al., 2020), which is supported by the geostatistical and microscopic observations above. The fluid flow is more likely to dissolve along the wider fractures and sliding surfaces in the fault core, and the dissolution phenomenon in the damage zone is obviously weaker compared to that in the fault core, causing the difference in the pore structure of carbonate rocks which eventually leads to strong heterogeneity for petrophysical and elastic properties. Thus, main factors affecting the heterogeneity of the studied carbonate strike-slip fault zone include the influence of fault structure position on fracture development, fluid selective filling on effective fracture and pore development, and the dissolution sequence on pore development.

Combining the geostatistical, microscopic observation and previous studies (Wu et al., 2019; Duan et al., 2020; Tang et al., 2021), we propose a simple fluid dissolution sequence controlling the development of vugs in the fault zone, which is associated with the complex diagenesis processes such as tectonic action and fluid activities. Firstly, the small

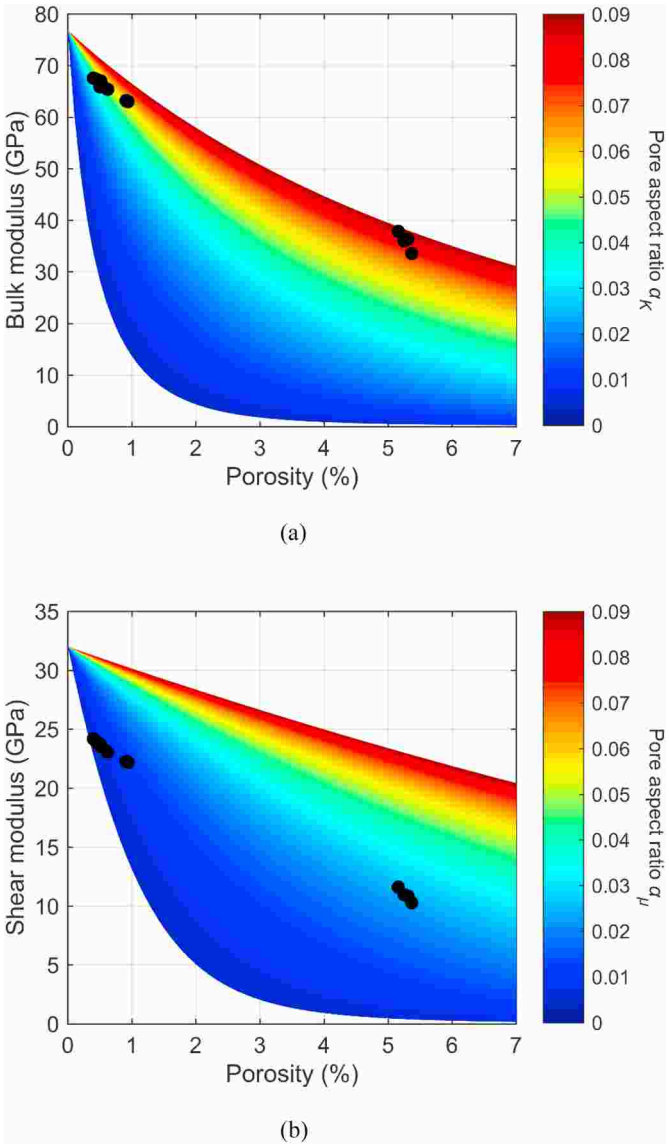

Fig. 13. The equivalent pore aspect ratio inversion template calculated based on DEM theory, the points are obtained by the P- and S- wave velocities and the density of the core samples.

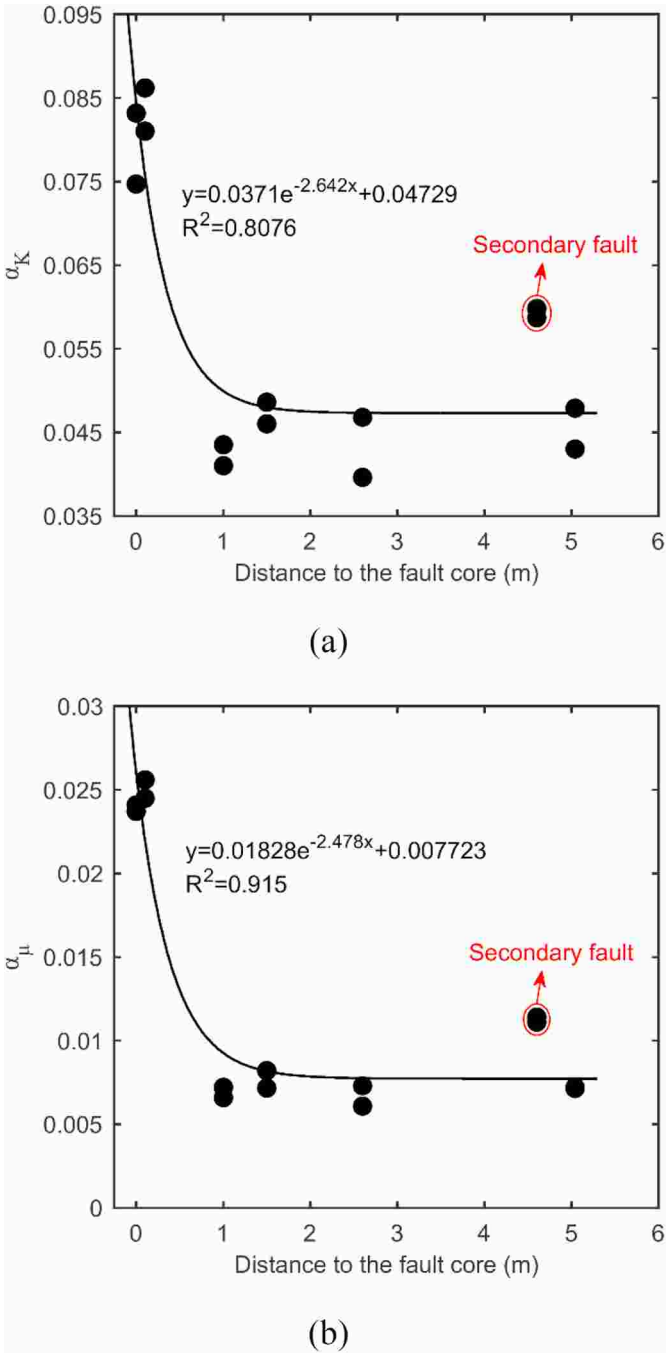

Fig. 14. The equivalent pore aspect ratios variations of the core samples drilled from different distance to the fault core.

dissolution pores are formed at the connection between the sliding surface and the fractures. And then, the dissolution pores are further expanded in the evolution process, the connectivity of the sliding surface and the fractures are increased, and the dissolution pores are gradually superimposed and connected to form the larger dissolved pores as shown in Fig. 15a and b. Finally, with the evolution of the fault zone and the continuous fluid action, the pores in the main fault continue to be overlapped and connected forming visible vugs, and the fluid also began to flow through the fractures in the damage zone, forming dissolution pores in this process as shown in Fig. 15c.

Although a small carbonate strike-slip fault zone is selected in this study, but the whole region for fault zone including the main fault core and fractured damage zone is investigated. Thus, the results in this paper provide important data and are helpful for recognition and prediction of the petrophysical and elastic properties and hydrocarbon exploration in carbonate strike-slip fault zone in the Tarim Basin. The results also can help us to understand the heterogeneity of petrophysical and elastic properties in carbonate strike-slip fault zone, and can provide reference for the construction of integrate multiscale heterogeneities models. In the future, one may need to conduct similar investigation by combining the geostatistical, cores, logging and 3D seismic data on hydrocarbon region in the Tarim Basin.

6. Conclusions

A small carbonate strike-slip fault zone is selected to investigate the heterogeneity of petrophysical and elastic properties, which are located in Yangjikan section in the Tarim basin, China. Based on the geostatistical, microscopic observation, petrophysical and ultrasonic analyses, and theoretical inversion, we can summarize the main scientific findings in this study.

The studied carbonate strike-slip fault zone mainly develops secondary pores dominated by solution pores, vugs and fractures. Both the

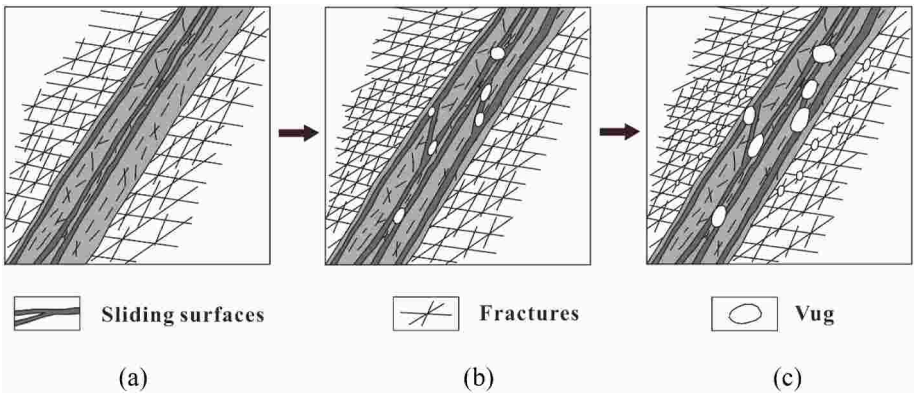

Fig. 15. Schematic diagram of fluid dissolution sequence controlling pores development in the fault zone.

macro- and micro-fractures features differ with the distance to the fault core, the fractures are most developed at the fault core, which are mainly fully filled or semi filled with calcite vein for the fault core but fully filled for the damage zone.

The petrophysical and elastic properties show significant complexities and heterogeneities, there are obvious differences between the values measured from two cores drilled from the same outcrop, especially for the samples from the fault core. The porosities and permeabilities of the samples drilled from the fault core are much times larger than those drilled from the damage zone. Both P-and S-wave velocities generally increase with the distance to the fault core, and the S- wave velocity is more sensitive to the distance.

The equivalent pore aspect ratio α_K and α_μ is derived from effective medium theory, both of them decrease with the distance to the main fault core, and the values for the fault core are much higher than those for the damage zone. The equivalent pore aspect ratio can be considered as relevant parameters for distinguishing the pore network architectures in carbonate rocks, and can provide references for the boundary identification of fractured damage zone.

The key factors controlling heterogeneity of petrophysical and elastic properties for the strike-slip carbonate fault zone mainly include the influence of fault structure position on fracture development, fluid selective filling on effective fracture and pore development, and the dissolution sequence on pore development.

Credit author statement

Fei Gong: Resources, Conceptualization, Methodology, Writing – original draft, Writing – review & editing. Yicheng Song: Data curation, Software. Lianbo Zeng: Project administration, Supervision, Funding acquisition. Guangui Zou: Validation, Data curation, Writing – review & editing.

Declaration of competing interest

The authors declare that they have no known competing financial interests or personal relationships that could have appeared to influence the work reported in this paper.

Data availability

The data that has been used is confidential.

Acknowledgements

This study is supported by the National Natural Science Fund Projects (U21B2062), the National Natural Science Fund Projects (42104107), the Fundamental Research Funds for the Central Universities (2022XJDC06), the National Key Research and Development Program of China (2018YFC0807803). The data associated with this research are available and can be obtained by contacting the corresponding author.

References

Abdlmutalib, A., Abdullatif, O., Abdelkarim, A., et al., 2019. Factors influencing acoustic properties of carbonate rocks: examples from middle Jurassic carbonates, Central Saudi Arabia. J. Afr. Earth Sci. 150, 767–782.
Agosta, F., Prasad, M., Aydin, A., 2007. Physical properties of carbonate fault rocks, fucino basin (Central Italy), Implications for fault seal in platform carbonates. Geofluids 7 (1), 19–32.
Berg, B.V., Nussbaumer, C., Noack, A., et al., 2017. A comparison of the relationship between measured acoustic response and porosity in carbonates across different geologic periods, depositional basins, and with variable mineral composition. Interpretation 6 (2), 245–256.
Bossennec, C., Géraud, Y., Moretti, I., et al., 2018. Pore network properties of sandstones in a fault damage zone. J. Struct. Geol. 110, 24–44.
Choi, J.H., Edwards, P., Ko, K., et al., 2016. Definition and classification of fault damage zones: a review and a new methodological approach. Earth Sci. Rev. 152, 70–87.
Choquette, P.W., Pray, L.C., 1970. Geologic nomenclature and classification of porosity in sedimentary carbonates. AAPG (Am. Assoc. Pet. Geol.) Bull. 54 (2), 207–250.
Couto, D.C.C., Barbosa, P.F., Santos, R.V., et al., 2021. Mineralogy composition and texture indicative of fluid-assisted remobilization in carbonate units of the Irece Basin, Brazil. J. S. Am. Earth Sci., 103346
Duan, T.Z., Zhang, W.B., Lu, X.B., et al., 2020. Architectural characterization of Ordovician fault-controlled paleokarst carbonate reservoirs, Tahe oilfield, China. Interpretation-A Jouranal of Subsurface Characterization 8 (4), 953–965.
Ferraro, F., Agosta, F., Prasad, M., et al., 2020. Pore space properties in carbonate fault rocks of peninsular Italy. J. Struct. Geol. 130, 103913.
Fournier, F., Leonide, P., Biscarrat, K., et al., 2011. Elastic properties of microporous cemented grainstones. Geophysics 76 (6), 211–226.
Fournier, F.M., Pellerin, M., Villeneuve, Q., et al., 2018. The equivalent pore aspect ratio as a tool for pore type prediction in carbonate reservoirs. AAPG (Am. Assoc. Pet. Geol.) Bull. 102, 1343–1377.
Garia, S., Pal, A.K., Ravi, K., et al., 2021. Laboratory assessment on factors controlling the acoustic properties of carbonates: a case study from Bombay offshore. J. Petrol. Sci. Eng. 203, 108607.
Geng, F., Wang, H.X., Hao, J.L., et al., 2021. Internal structure characteristics and formation mechanism of reverse fault in the carbonate rock, A case study of outcrops in xike'er area, Tarim basin, northwest China. Front. Earth Sci. 9, 793016.
Guo, R.X., Zhang, S.N., Bai, X.L., et al., 2020. Hydrothermal dolomite reservoirs in a fault system and the factors controlling reservoir formation-A case study of Lower Paleozoic carbonate reservoirs in the Gucheng area, Tarim Basin. Mar. Petrol. Geol. 120, 104506.
Jeanne, P., Guglielmi, Y., Lamarche, J., et al., 2012a. Architectural characteristics and petrophysical properties evolution of a strike-slip fault zone in a fractured porous carbonate reservoir. J. Struct. Geol. 44, 93–109.
Jeanne, P., Guglielmi, Y., Cappa, F., 2012b. Multiscale seismic signature of a small fault zone in a carbonate reservoir: relationships between V-P imaging, fault zone architecture and cohesion. Tectonophysics 554, 185–201.
Jiu, B., Huang, W.H., Li, Y., 2020. The Effect of Hydrothermal Fluids on Ordovician Carbonate Rocks, Southern Ordos Basin, China. Ore Geology Reviews, p. 103803.
Kenter, J., Braaksma, H., Verwer, K., et al., 2007. Acoustic behavior of sedimentary rocks: geologic properties versus Poisson's ratios. Lead. Edge 26 (4), 436–444.
Kuster, G.T., Toksoz, M.N., 1974. Velocity and attenuation of seismic-waves in two-phase media, Part II. Experimental results. Geophysics 39 (5), 607–618, 1974.
Leonide, P., Borgomano, J., Masse, J.P., et al., 2012. Relation between stratigraphic architecture and multi-scale heterogeneities in carbonate platforms: the Barremian-lower Aptian of the Monts de Vaucluse, SE France. Sediment. Geol. 265, 87–109.
Lønøy, A., 2006. Making sense of carbonate pore systems. AAPG (Am. Assoc. Pet. Geol.) Bull. 90 (9), 1381–1405.

Ma, Y.S., Cai, X.Y., Yun, L., et al., 2022. Practice and theoretical and technical progress in exploration and development of Shunbei ultra-deep carbonate oil and gas field, Tarim Basin, NW China. Petrol. Explor. Dev. 49 (1), 1–20.
Manoorkar, S., Jackson, S.J., Krevor, S., 2021. Observations of the impacts of millimeter-to centimeter-scale heterogeneities on relative permeability and trapping in carbonate rocks. Water Resour. Res. 57, e2020WR028597.
Matonti, C., Lamarche, J., Guglielmi, Y., et al., 2012. Structural and petrophysical characterization of mixed conduit/seal fault zones in carbonates: example from the Castellas fault (SE France). J. Struct. Geol. 39, 103–121.
Mavko, G., Mukerji, J., Dvorkin, J., 2003. The Rock Physics Handbook, Tools for Seismic Analysis in Porous Media. Cambridge University Press, New York, pp. 1–329.
Méndez, J.N., Jin, Q., Gonzalez, M., et al., 2020. Fracture characterization and modeling of karsted carbonate reservoirs: a case study in Tahe oilfield, Tarim Basin (western China). Mar. Petrol. Geol. 112, 104104.
Mercuri, M., Carminati, E., Tartarello, M.C., et al., 2020. Lithological and structural control on fracture frequency distribution within a carbonate-hosted relay ramp. J. Struct. Geol. 137, 104085.
Michie, E.A.H., Haines, T.J., 2016. Variability and heterogeneity of the petrophysical properties of extensional carbonate fault rocks, Malta. Petrol. Geosci. 22 (2), 136–152.
Mitchell, T.M., Faulkner, D.R., 2009. The nature and origin of off-fault damage surrounding strike-slip fault zones with a wide range of displacements: a field study from the Atacama fault system, northern Chile. J. Struct. Geol. 31 (8), 802–816.
Norris, A.N., 1985. A differential scheme for the effective moduli of composites. Mech. Mater. 4 (1), 1–16.
O'Hara, A.P., Jacobi, R.D., Sheets, H.D., 2017. Predicting the width and average fracture frequency of damage zones using a partial least squares statistical analysis: implications for fault zone development. J. Struct. Geol. 98, 38–52.
Pan, J.G., Wang, H.B., Li, C., et al., 2015. Effect of pore structure on seismic rock-physics characteristics of dense carbonates. Appl. Geophys. 12 (1), 1–10.
Pan, J.G., Deng, J.X., Chuang, L., et al., 2019. Effects of micrite microtextures on the elastic and petrophysical properties of carbonate reservoirs. Appl. Geophys. 16 (4), 399–413.
Petunin, V.V., Yin, X., Tutuncu, A.N., 2011. Porosity and permeability changes in sandstones and carbonates under stress and their correlation to rock texture. In: Canadian Unconventional Resources Conference. https://doi.org/10.2118/147401-MS.
Qi, L.X., 2021. Structural characteristics and storage control function of the Shun I fault zone in the Shunbei region, Tarim Basin. J. Petrol. Sci. Eng. 203, 108653.
Smeraglia, L., Mercuri, M., Tavani, S., et al., 2021. 3D Discrete Fracture Network (DFN) models of damage zone fluid corridors within a reservoir-scale normal fault in carbonates: multiscale approach using field data and UAV imagery. Mar. Petrol. Geol. 126, 104902.
Tang, Y., Zhang, Y.F., Tang, H.M., et al., 2021. Carbonate burial dissolution related to faults and fractures in the triassic daye formation of the huandiqiao section, huangshi area, hubei, China. Can. J. Earth Sci. 58 (1), 38–49.
Tian, F., Di, Q.Y., Jin, Q., et al., 2019. Multiscale geological-geophysical characterization of the epigenic origin and deeply buried paleokarst system in Tahe Oilfield, Tarim Basin. Mar. Petrol. Geol. 102, 16–32.
Torabi, A., Alaei, B., Ellingsen, T.S.S., 2018. Faults and fractures in basement rocks, their architecture, petrophysical and mechanical properties. J. Struct. Geol. 117, 256–263.
Verwer, K., Braaksma, H., Kenter, J.A.M., 2008. Acoustic properties of carbonates: effects of rock texture and implications for fluid substitution. Geophysics 73 (2), 51–65.
Wang, Z.Z., Wang, R.H., Wang, F.F., et al., 2015. Experiment study of pore structure effects on velocities in synthetic carbonate rocks. Geophysics 80 (3), 207–219.
Wang, Q.L., Han, J.F., Li, H., et al., 2019. Carbonate sequence architecture,sedimentary evolution and sea level fluctuation of the Middle and Lower Ordovician on outcrops at the northwestern margin of Tarim Basin. Oil Gas Geol. 40 (4), 835–850.
Wang, Z.Y., Gao, Z.Q., Fan, T.L., et al., 2020. Structural characterization and hydrocarbon prediction for the SB5M strike-slip fault zone in the Shuntuo Low Uplift, Tarim Basin. Mar. Petrol. Geol. 117, 104418.
Wang, Z., Gao, Z., Fan, T., Zhang, H., Qi, L., Yun, L., 2021. Hydrocarbon-bearing characteristics of the SB1 strike-slip fault zone in the north of the Shuntuo low uplift. Tarim Basin. Petrol. Geosci. 27 (1).
Wei, C., Cheng, S.Q., Chen, G., et al., 2021. Parameters evaluation of fault-karst carbonate reservoirs with vertical beads-on-string structure based on bottom-hole pressure, Case studies in Shunbei Oilfield, Tarim Basin of Northwestern China. Oil & Gas Science and Technology – Revue d'IFP Energies nouvelles 76, 59.
Wennberg, O.P., Casini, G., Jahanpanah, A., et al., 2013. Deformation bands in chalk, examples from the shetland group of the oseberg field, north sea, Norway. J. Struct. Geol. 56 (7), 103–117.
Wu, G.H., Gao, L.H., Zhang, Y.T., et al., 2019. Fracture attributes in reservoir-scale carbonate fault damage zones and implications for damage zone width and growth in the deep subsurface. J. Struct. Geol. 118, 181–193.
Wu, G., Zhao, K.Z., Qu, H.Z., et al., 2020. Permeability distribution and scaling in multi-stages carbonate damage zones: insight from strike-slip fault zones in the Tarim Basin, NW China. Mar. Petrol. Geol. 114, 104208.
Xu, X.Y., Chen, Q.H., Zhang, Y.G., et al., 2021. Research progress and prospect of Ordovician carbonate rocks in Tahe oilfield: karst feature. J. Pet. Explor. Prod. Technol. 11 (11), 3889–3902.
Zeng, L.B., Jiang, J.W., Yang, Y.L., 2010. Fractures in the low porosity and ultra-low permeability glutenite reservoirs: a case study of the late Eocene Hetaoyuan formation in the Anpeng Oilfield, Nanxiang Basin, China. Mar. Petrol. Geol. 27 (7), 1642–1650.
Zhang, W.B., Duan, T.Z., Li, M., et al., 2021. Architecture characterization of Ordovician fault-controlled paleokarst carbonate reservoirs in Tuoputai,Tahe oilfield,Tarim Basin,NW China. Petroleum Exploration and Development Online 48 (2), 314–325.
Zhao, L.X., Geng, J.H., Cheng, J.B., et al., 2014. Probabilistic lithofacies prediction from prestack seismic data in a heterogeneous carbonate reservoir. Geophysics 79 (5), 25–34.
Zhao, H.T., Wang, Z.Q., Liu, J., 2016. Main diagenesis of middle-lower ordovician of yubei area in Tarim basin. Earth Sci. 8 (6), 352–358.
Zhao, L.X., Cao, C.H., Yao, Q.L., et al., 2020. Gassmann consistency for different inclusion-based effective medium theories: implications for elastic interactions and poroelasticity. J. Geophys. Res. Solid Earth 125 (3), e2019JB018328.
Zhou, X.G., Du, Z.L., 2019. Progress and achievements in oil and gas geological survey and exploration of new strata in new area of Northern China. Geological Survey of China 6 (4), 1–10.